




A novel hybrid strip finishing process to improve mechanical properties and reduce energy consumption

Alpha Pernia-Espinoza¹  · Volker Diegelmann² · Ruben Escribano-Garcia¹ · Julio Fernandez-Ceniceros¹ · F. Javier Martinez-de-Pison¹

Received: 1 September 2017 / Accepted: 8 January 2018 / Published online: 29 January 2018
© Springer-Verlag France SAS, part of Springer Nature 2018

Abstract

The growing demand for new steel grades, such as high formability steels and high or ultra-high strength steels for structural and safety-related automotive components, make manufacturing steel sheets an increasingly complex task. A novel hybrid process (HyP), that combines the skin-pass and tension levelling processes into one production step is proposed to improve the steel strip manufacturing chain. The HyP applies asymmetrical rolling (H-ASR) by using different roll diameters and by bending the strip before it enters the roll gap. The potential advantages of H-ASR, such as the introduction of through-thickness higher plastic deformation and the use of reduced roll force and power, were investigated by means of elastic-plastic finite element models and experimental data. The numerical models were validated by experiments at a HyP pilot facility and by industrial trials. Analytical estimation of the appropriate bending limits was included. The contact condition, material deformation and stress state during rolling were analysed and compared with the results of a conventional skin-pass process. It was verified that the proposed H-ASR introduced higher shear deformation throughout the strip thickness than a traditional skin-pass process. The positive influence of this fact was verified by tensile and formability tests on material processed by the HyP pilot facility. The results indicate that the HyP produces sheets with better drawability, satisfactory strength, and formability qualities comparable to those of the conventional finishing processes. What's more, the HyP boasts all these advantages while using a space-saving layout and reducing energy consumption as compared to traditional finishing processes.

Keywords Skin-pass · Tension-levelling · Asymmetric rolling · Mechanical properties · Finite element

Introduction

The development of new steel grades, such as high formability steels and high or ultra-high strength steels for structural or safety-related automotive components, demands new approaches to manufacturing steel sheets [1]. At present, the finishing stage of the cold-rolled steel strip manufacturing process comprises the skin-pass and tension levelling processes. Skin-pass is applied to annealed strips to fulfil two main objectives: eliminate yield point elongation and provide the strip with a specific roughness. The process primarily consists of slightly reducing the sheet thickness (up to 2%) by applying compression forces through two similar rolls, namely work rolls. When yield point elongation is eliminated, potential Lüder's bands, with their derived sheet surface defects, are also avoided in further transformation processes [2]. The subsequent tension levelling process is widely employed to reduce residual stresses and guarantee strip flatness for shape-

✉ Alpha Pernia-Espinoza
alpha.pernia@unirioja.es

Volker Diegelmann
Volker.Diegelmann@bfi.de

Ruben Escribano-Garcia
ruben.escribano@unirioja.es

Julio Fernandez-Ceniceros
julio.fernandezc@unirioja.es

F. Javier Martinez-de-Pison
fjmartin@unirioja.es

¹ EDMANS Research Group, Department of Mechanical Engineering, Edificio Departamental, University of La Rioja, C/ Luis de Ulloa 20, 26004 Logroño, La Rioja, Spain

² VDEh-Betriebsforschungsinstitut, Surface Technology, Sohnstrasse 65, 40237 Düsseldorf, Germany

critical post-processing [3]. This is achieved by alternately bending the strip around small diameter rolls subjected to significant longitudinal tension. Thus, shape defects are removed by fibre-length equalization.

Nevertheless, in the skin-pass process, several problems can arise depending on the material strength and surface texture requirements. High strength materials require great force to overcome yield point elongation and also to make roughness transfer possible. On the other hand, low-strength steels demand low deformation to attain the optimum elongation capability, and at the same time high work roll force to achieve the roughness transfer requirement. Given these circumstances, any solution must address both of these conflicting requirements. And furthermore, applying high work roll force to the strip increases roll wear which decreases the roll's service life. In addition, the greater the roll force, the greater the possibility of encountering shape defects such as waviness [4].

With these issues in mind, a new strip finishing process was developed as part of a project funded by the European Union (RFSR-CT-2007-00016). A general explanation is presented in [5]. This process, named *hybrid process* (HyP), combines skin-pass and tension levelling into one production step. Two cycles of the tension-levelling-rolling-arrangement and two textured work rolls opposite one another constitute the HyP (Fig. 1). As can be observed in Fig. 1, the HyP applies asymmetrical rolling (ASR) over the strip in two steps (module 1 and module 2). From this point on, H-ASR is used to refer to the ASR introduced by the HyP. Two types of ASR occur at each module: geometrical, as the diameters of the compressive rolls are different; and tribological, as the compressive rolls have different surface textures [6]. In addition, a superimposed bending under tension is applied, contributing to the geometrical asymmetry during the rolling process. In this way, the intended functionalities of the HyP were to facilitate the roughness transfer by bending the strip (producing outer fibre stress state close to the yield point) and at the same time, obtain the desired elongation and mechanical properties using reduced roll force.

ASR has been proven to have several advantages over symmetrical rolling (SR): it reduces rolling force and, when using some types of ASR, torque is also reduced [7–11]. It also introduces extra shear deformation through the strip thickness which has a great influence on the final microstructure and texture, and therefore on the mechanical and formability properties of the processed material [8, 12]. ASR has been introduced in different ways and has been successfully incorporated to process several different materials. Hwang, Tzou [7] and Ouali, Aberkane [13] studied the effect of using different rolls diameters in processing aluminium alloys. Cai et al. [14] used the same ASR principle to process low carbon microalloyed steel. ASR by bending the strip before rolling was proposed by Ma et al. [15] for the manufacture of magnesium alloys. Toth et al. [16] analysed ASR using one idle

roll in processing interstitial-free (IF) steel. Hamad et al. [17] also study ASR processing of IF steel, but in this case by using different peripheral rolls speeds. The same ASR principle was also applied by [1] on stainless steel and by [13] on aluminium. Recently, an ASR approach called *snake rolling* that combines different rolls' peripheral velocities with horizontally-displaced roll centres was successfully applied to aluminium alloys [10, 18–20]. In most of these studies numerical simulations using the finite element method (FEM) were conducted, which has proved to be an excellent tool for the analysis of symmetric [21–24] and asymmetric rolling.

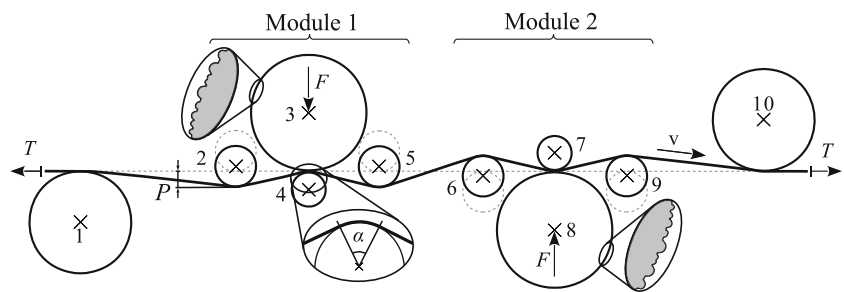
In the present study the proposed HyP is described and the potential advantages of the H-ASR, such as the introduction of through-thickness higher plastic deformation and reduced roll force and power, are investigated. Contact condition, material deformation and stress state during rolling in the HyP are analysed and compared to the traditional skin-pass process by means of 2D elastic-plastic FEM models. The validation of the FEM models using experimental data obtained from a HyP pilot facility and industrial trials is also reported. The material in question is the mild steel DC04, usually employed for cold forming. The influence of introducing through-thickness shear deformation during H-ASR was verified by tensile and formability tests. The roll force and power employed to attain the desired elongation and the mechanical and formability properties of the processed material are compared to the corresponding results of the conventional processes in equivalent conditions.

The hybrid process (HyP)

HyP configuration and parameters

The HyP incorporates two modules which alternatively bend the strip and transfer texture to a specific part of the sheet (Fig. 1): module 1 transfers texture to the upper part; and module 2, to the bottom portion of the strip. Work rolls 3 and 8 are those that have the surface structure to be transferred, by means of the roll force (F). Support rolls 4 and 7, in combination with bending rolls 2 and 5 for module 1, and 6 and 9 for module 2, alternatively bend the strip. These rolls generate the effects of tension levelling, producing two bending cycles on the strip. The bending rolls (2, 5, 6, and 9) can pivot around their corresponding work roll centre, to a defined vertical position or penetration (P), allowing the wrap angle (α) to be varied. The wrap angle is defined as the angle subtended by the radii of the extreme strip-support roll contact points. In addition, the sheet is submitted to a lengthwise tension (T), which also influences the α value. The strip moves at a constant velocity (v), imposed by downstream and upstream processes. In this research, the pilot facility used to investigate the basic principles of the HyP utilises non-driven rolls. Thus, rolls 2 through 9 are not driven, i.e.

Fig. 1 HyP: general configuration



they move by means of friction between sheet and rolls. The necessary lengthwise tension along the process is applied by the bridle rolls (rolls 1 and 10). Nevertheless, on an industrial scale, the HyP would probably require driven work rolls.

In order to process a strip in the HyP, it is first submitted to the desired lengthwise tension (T). Then, bending rolls 2, 5, 6 and 9 pivot around the corresponding work rolls, to a predefined penetration (P), bending the strip to the corresponding wrap angle (α). Roll force (F) is applied afterwards and finally the strip is moved forward (from left to right in Fig. 1) at a target constant velocity (v). Therefore, the parameters that could be adjusted in the HyP are those traditionally adjusted in conventional skin-pass and tension-levelling processes: roll force (F), lengthwise tension (T) and penetration (P). Nevertheless, these parameters can now act simultaneously (though each of them can be adjusted separately) to improve the final product. That is, the wrap angle, as an essential part of the levelling component of the HyP, can be modified while the material is skin passed. And inversely, the roll force, as the fundamental variable of the skin pass component of the HyP, can be varied while the material is undergoing the levelling process.

Another positive aspect of the HyP is the space required for its industrial implementation. It is expected that 25% to 30% less space would be needed than for a typical finishing layout (consisting of a skin-pass and a two-cycle tension levelling processes).

Analytical estimation of bending limits

In order to facilitate imprinting any kind of roughness, the strip’s surface must reach the roll gap in a state close to yielding. If the material is already in a more plastic state when entering the roll gap, the work-hardening would hinder the roughness transfer. Once in the roll gap, the necessary roll force also depends on the required degree of roughness transfer. Therefore, bending limits should be stated in order to guarantee adequate roughness transfer using minimum roll force.

As the strip width is much greater than its thickness and the spread in the transverse direction is neglected, the HyP is treated as a plane strain problem. The material behaviour before the roll gap can be analysed as it has been processed by a common tension-levelling process. According to Marciniak

et al. [25], a strip bent around a roll under superimposed tension, presents a longitudinal strain (ϵ_x) at a distance y from the strip central axis given by Eq. (1):

$$\epsilon_x = \epsilon_a + \epsilon_b = \frac{\beta}{\rho} + \frac{y}{\rho} = \frac{\beta + y}{\rho} \tag{1}$$

where ϵ_a is the strain at the strip’s central axis ($\epsilon_a = \beta/\rho$), ϵ_b is the bending strain ($\epsilon_b = y/\rho$), β is the displacement of the neutral axis from the central axis (which is produced by the applied lengthwise tension on the bent strip) and ρ is the bend radius of the central axis. Roberts, Sheppard [26] generalized Eq. (1) for successive bending using Eq. (2).

$$\epsilon_{x_i} = \frac{(\pm y + \beta_i)}{\rho} (1 + \epsilon_{x_{i-1}}) \tag{2}$$

The equilibrium of forces over a unit width of section can be expressed by Eq. (3).

$$\sigma_{lw} \cdot h = \int_{-\beta}^{h/2} \sigma_x dy - \int_{-h/2}^{-\beta} \sigma_x dy \tag{3}$$

where σ_{lw} is the actual lengthwise tension and h is the strip’s thickness. Assuming that the material has just reached yielding at both surfaces, i.e. $\sigma_x = S$, where S is the plane strain yield stress ($S = \frac{2}{\sqrt{3}} \cdot \sigma_y$), β can be obtained using Eq. (4).

$$\beta = (h \cdot \sigma_{lw}) / (2 \cdot S) \tag{4}$$

Thus, the neutral axis displacement is directly proportional to the applied lengthwise tension and inversely proportional to the material yield stress.

The limit of *elastic bending* is defined as when the strip’s outer surface ($y = h/2$) reaches the plane strain yield stress S . Therefore, the limiting elastic strain is given by $\epsilon_e = S/E'$, where E' is the plane strain elastic modulus ($E' = E/(1-\nu^2)$). From Eq. (1), the *limiting elastic radius of curvature* can be obtained using Eq. (5).

$$\rho_e = \frac{\left(\frac{h}{2} + \beta\right) E'}{S} \tag{5}$$

Therefore, in order to assure plasticity, the radius of curvature should be lower than ρ_e .

Once in the *plastic bending* stage, the material behaviour can be approximated by the strain-stress relationship obtained in the tensile test: $\sigma_x = A(B + \varepsilon_x)^m$. As before, the strain is given by $\varepsilon_x = \varepsilon_a + \varepsilon_b = \frac{\beta}{\rho} + \frac{\beta}{\rho}$. According to Marciniak et al. [25], the stress-strain relation can be assumed to be linear in a limited strain range, with a slope of $d\sigma_x/d\varepsilon_x|_{\varepsilon_{x_i}}$, where ε_{x_i} is the centre of the considered strain range. Therefore, the corresponding stress is given by Eq. (6).

$$\sigma_x = \sigma_a + \left. \frac{d\sigma_x}{d\varepsilon_x} \right|_{\varepsilon_{x_i}} \cdot \frac{y}{\rho} \tag{6}$$

where σ_a is the stress at the central axis, expressed by $\sigma_a = A(B + \varepsilon_a)^m$.

Considering a desired increment on plane strain yield stress ($\Delta S\%$) at the strip’s surface ($y = h/2$), Eq. (5) leads to Eq. (7).

$$(1 + \Delta S\%) \cdot S = A \left(B + \frac{\beta}{\rho_f} \right)^m + m \cdot A \left(B + \frac{\beta + h/2}{\rho_f} \right)^{m-1} \cdot \left(\frac{h/2}{\rho_f} \right) \tag{7}$$

where ρ_f is the corresponding radius of curvature for the desired plastic state or the *limiting plastic radius of curvature*. ρ_f can be obtained using a Nelder and Mead iteration algorithm [27].

Hence, in order to ensure an adequate plastic state during rolling by the HyP, the radius of curvature should be lower than ρ_e and higher than ρ_f (Eq.(8)).

$$\rho_f < \rho < \rho_e \tag{8}$$

Experimental procedure and FEM modelling

Pilot plant and industrial trials

For the practical implementation of the HyP, a tension levelling facility at BFI (Betriebsforschungsinstitut GmbH, Düsseldorf-Germany) was reconstructed (Fig. 2). The result was a compact finishing machine, combining both processes: skin-pass and tension levelling.

The barrel width was 400 mm. The diameter of the bending rolls 2, 5, 6 and 9 was 100 mm. Support rolls 4 and 7 measured 80 mm in diameter, and incorporated two back-up rolls with a diameter of 90 mm to support radial force components. The diameters of the work rolls 3 and 8 were 300 mm, with bearing assemblies designed to apply normal forces (F) by means of a hydraulic unit (of 200 kN). Therefore, the work roll/support roll diameter ratio was equal to 3.75. During trials in the pilot plant, lengthwise tension was defined as a percentage of the steel’s yield stress (σ_{x_0}): $T = 100 \cdot (\sigma_{tw} / \sigma_{x_0})$, where σ_{tw} is the actual

lengthwise tension applied to the strip. In the pilot facility σ_{tw} could be varied to a maximum of 350 MPa. Bending roll penetration (P) could be varied from 0 to 60 mm. Roll force (F) could be varied to a maximum of 200 kN. These wide ranges of the parameters allow the facility to process low, mild and high strength steels. Strip velocity was set to 2.4 m/min, thanks to the facility’s uncoiling and coiling system. The applied roll force was detected by a digital pressure sensor. A tension-measuring roll was installed to measure lengthwise tension. Also, a digital angular devise was installed to measure the wrap angle. Regarding elongation (e), the strip was marked in the longitudinal direction, and distances between marks were measured before and after the process using a micrometre. The relationship used to calculate it was: $e = 100 \cdot (e_f - e_0) / e_0$ where e_0 and e_f are the initial and final distances between marks, respectively. The material processed during this study was the low strength steel DC04 (EN 10130). The entry material properties are summarised in Table 1.

The experiments to validate the FEM models (Table 2) were performed according to the central composite design (CCD) [28]. Since the processed material was mild strength steel (DC04), the ranges for the HyP parameters, T , P and F , were set to: 10 to 30% σ_{x_0} , 6 to 18 mm and 100 to 200 N/mm, respectively, following the recommendations of Sections “Analytical estimation of bending limits and Bending limits”. The trials involving the conventional manufacturing process (by means of tension levelling and skin-pass processes) were conducted in an industrial facility at the Bilstein Group Hagen’s plant. The conditions were similar to those at the HyP pilot plant (work roll diameters, velocity, strip’s entry properties, etc.). Each trial was conducted at least three times and the results presented herein correspond to the average values. All trials were conducted in dry conditions.

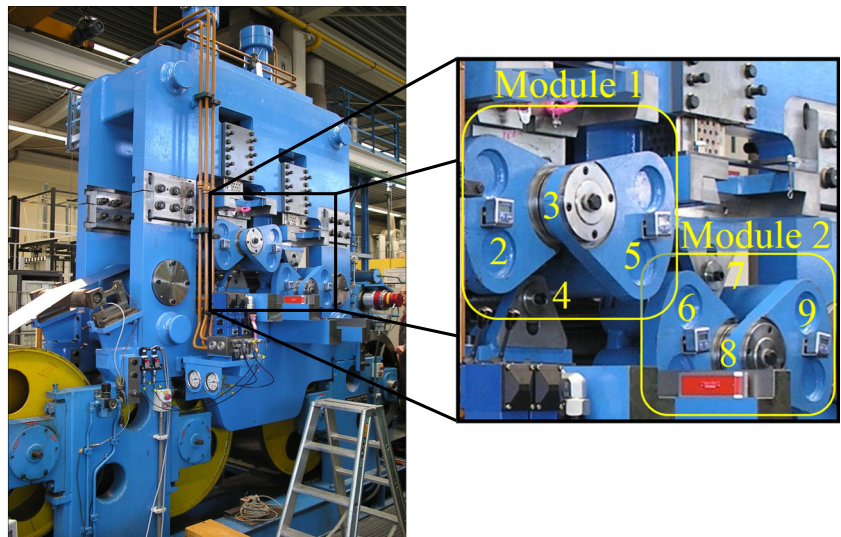
In Fig. 3 some of the HyP pilot facility trials are presented.

The skin-pass industrial trials are depicted in Fig. 4.

FEM model

During the HyP, the steel strip is submitted to asymmetrical compression under tensional and bending loads. To analyse the contact condition, material deformation and stress characteristics under this load state, a two-dimensional plane strain FEM model was developed using the ABAQUS v 6.11 dynamic explicit method [29]. For the sake of simplicity, roughness transfer was not included in this analysis (the work roll was considered smooth), since the micro-deformations produced by the roughness structure would not significantly affect the results. Nevertheless, different Coulomb friction coefficients were set for the contacts’ work roll-strip (0.3) and support roll-strip (0.1) in order to account for differences in surface roughness. Tribology asymmetry, however, is not studied extensively in this work.

Fig. 2 HyP pilot facility, including a zoom identifying the modules and rolls as in Fig. 1 (photographs courtesy of BFI)



A preliminary study conducted with a simplified FEM model of the HyP, which included only module 1 and applied dynamic compression through elastic work roll and support roll, indicated a non-conventional elastic deformation of the work roll (which will be discussed in a further section) and a negligible elastic deformation at the support roll. Consequently, a deformable body was adopted for the work-roll modelling and rigid bodies for the modelling of support and bending rolls (Fig. 5). The steel strip was modelled as an elasto-plastic material through a kinematic hardening model. Regarding the meshing, the sheet was split into three areas in order to reduce the analysis burden: one fine mesh area (study area), surrounded by two coarse mesh areas (Fig. 5). Different element sizes were tested and the final mesh size was chosen taking into consideration accuracy and computational effort. The chosen mesh configuration was that with rectangular elements (CPE4R) with 1/16th the size of the strip thickness in the study area, and 1/3rd in the coarse mesh area. Transitional triangular elements (CPE3) were used to join the different areas.

Mechanical and formability properties

The mechanical properties of the entry material and final product were determined by tensile tests performed in an Instron

4507 universal testing machine, in accordance with standard EN10002–1. In order to evaluate anisotropy at the resulting sheet, specimens were cut along the rolling direction (RD) (0°), 45° from the RD and in the transverse direction (90°). At least three samples per test were taken. Since sheet metal under biaxial tension conditions can bear much higher strain levels (before local necking or fracture appearance) than under a uniaxial tensile test, bulge tests were conducted in order to evaluate formability. The forming limit curve (FLC), which limits strain during formability (to avoid fracture), was determined using the Zurich number 5 method, as recommended by the International Deep Drawing Research Group [30]. The

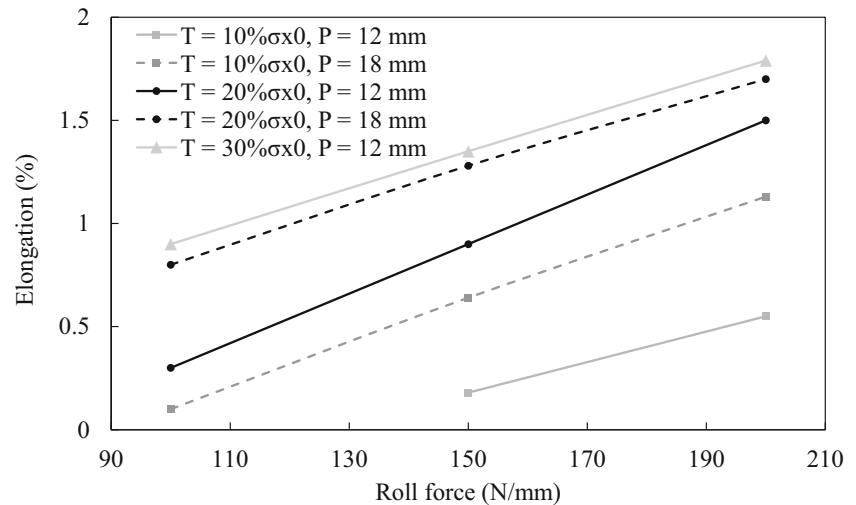
Table 1 DC04 material properties and strip dimensions

	DC04 strip (entry conditions)
Yield stress (σ_{x_0})	161 MPa
Elastic modulus (E)	210 GPa
Poisson’s ratio (ν)	0.3
Initial thickness (h_0)	1 mm
Initial width (w_0)	200 mm
Stress/strain relationship	$\sigma_x = 520 \cdot (0.0015 + \epsilon_x)^{0.18}$

Table 2 Trials at the HyP pilot facility

Trial	T (% σ_{x_0})	F (N/mm)	P (mm)	Final Elongation (%)
1	10	100	6	0.07
2	10	150	12	0.18
3	10	200	12	0.55
4	10	100	18	0.10
5	10	150	18	0.64
6	10	200	18	1.13
7	20	100	6	0.49
8	20	150	6	0.53
9	20	200	12	0.30
10	20	150	12	0.90
11	20	100	12	1.50
12	20	150	18	0.80
13	20	200	18	1.28
14	20	200	18	1.70
15	30	100	6	1.80
16	30	150	12	0.90
17	30	200	12	1.35
18	30	200	12	1.79

Fig. 3 Experimental relationship between rolling force and elongation for different lengthwise tensions and penetrations. Experimental data obtained from the HyP pilot facility



deformation of the sheet blanks was evaluated by means of three tests: tensile tests, a biaxial-circular (100 mm) test, and biaxial-elliptical (100/63 mm) tests. In order to incorporate another indicator of product formability, the Erichsen cupping test was also performed. The Erichsen index (IE) was calculated using the standard DIN 50101. All samples were cut at least 50 mm away from the strip peripherals in order to avoid the edge-effect.

Energy requirements calculation

The analysis of energy requirement was based on the roll force and power used by the HyP to achieve the same final elongation as the conventional finishing process.

Regarding the power required to deform the material along the roll gap, it can be obtained by means of the rolling torques, T_1 and T_2 , exerted by the sheet on the upper and bottom rolls, respectively. The rolling torques can be calculated by integrating

the moment of the shear friction forces along the contact length around the respective roll axis [7].

$$T_1 = R_1 \left(\int_{L_{11}}^{NP_1} \tau_1 dx + \int_{NP_1}^{NP_2} \tau_1 dx + \int_{NP_2}^{L_{21}} \tau_1 dx \right) \quad (9)$$

$$T_2 = R_2 \left(\int_{L_{12}}^{NP_1} \tau_2 dx + \int_{NP_1}^{NP_2} \tau_2 dx + \int_{NP_2}^{L_{22}} \tau_2 dx \right) \quad (10)$$

where R_1 and R_2 are the radius of the upper and bottom rolls, respectively; NP_1 and NP_2 are the horizontal positions of the first and second neutral points, respectively; L_{11} and L_{21} are the initial and final horizontal position of the upper contact length, respectively; L_{12} and L_{22} are the initial and final horizontal position of the bottom contact length, respectively; and τ_1 and τ_2 are the shear friction stresses along the upper and bottom roll surfaces, respectively. Relying on the verified numerical models, the interfacial shear stress curves obtained by the FEM models were integrated to obtain the rolling torques, T_1 and T_2 .

Fig. 4 Experimental relationship between rolling force and elongation for different lengthwise tensions. Data obtained from the skin-pass process industrial trials

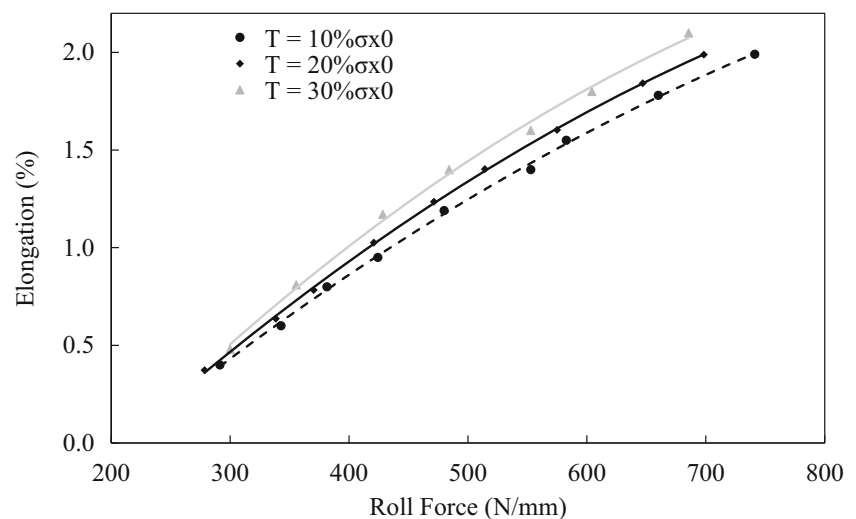
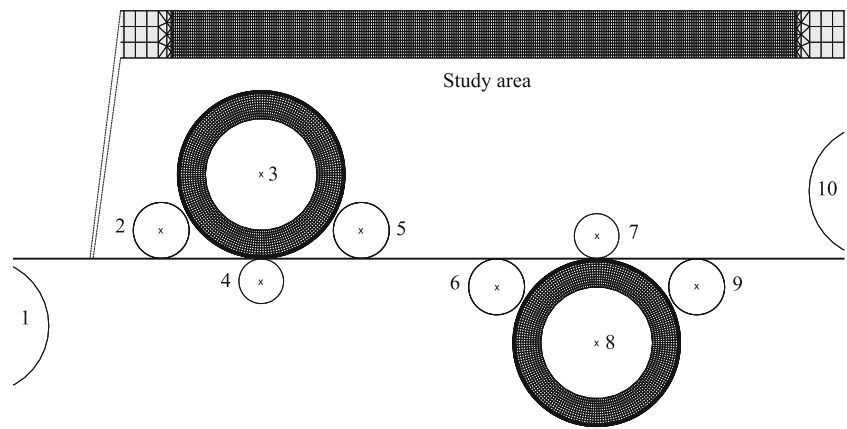


Fig. 5 FEM model assembly and zoom of strip meshing



Finally, the power required to deform the sheet can be calculated using Eqs. (11) and (12).

$$P_1 = T_1 \cdot \omega_1 \quad (11)$$

$$P_2 = T_2 \cdot \omega_2 \quad (12)$$

where P_1 and P_2 are the upper and bottom roll power, respectively; and ω_1 and ω_2 are the upper and bottom rolling angular velocities, respectively.

Results and discussion

Experimental relationship between rolling force and elongation

The relationship between rolling force and elongation follows a rectilinear tendency for the HyP (Fig. 3) and a slightly logarithmic tendency for the conventional skin-pass process (Fig. 4). Similar observations were made regarding the skin-pass process by Kijima, Bay [22]. Figure 3 also found that the three input variables (lengthwise tension, penetration and roll force) positively influenced elongation. A very important difference between the results of both processes is the value of the medium derivative of the change in elongation over rolling force, which is higher for the HyP (1.2%/(100 N/mm)) than for the skin-pass process (0.4%/(100 N/mm)).

Validation of FEM models

A reasonable agreement was achieved between experimental and simulated elongation for the HyP (Fig. 6a) with a root mean square error (RMSE) of 11% and a coefficient of determination (R^2) of 0.90. In addition, for the skin-pass process, the FEM model presented good agreement with the experimental trials, with a RMSE of 9% and a R^2 of 0.97 (Fig. 6b).

Bending limits

Using a Nelder and Mead iteration algorithm (NM-algorithm), ρ_f was obtained by means of Eq. (7) and for different lengthwise tensions. The results were verified using the FEM model. The comparison is displayed in Fig. 7, showing strong agreement between the calculated values and the FEM model results. The minimum ρ_f is limited by the bending roll radius (40 mm).

A summary of the values used in Eq. (7) and limiting radius of curvature, elastic (ρ_e) and plastic (ρ_f), for different lengthwise tensions are presented in Table 3. The corresponding bending roll penetration (P) is also included.

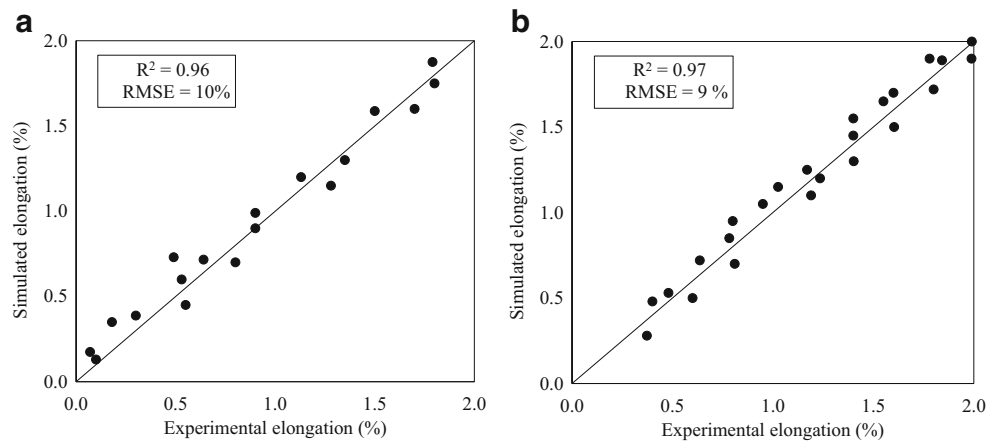
The parameters ranges for the trials at the HyP pilot facility provided in Section “Pilot plant and industrial trials” are in agreement with the values presented in Table 3. Thus, for medium values of the parameters (i.e. $T = 20\% \sigma_{x0}$, $F = 150$ N/mm and $P = 12$ mm), the corresponding increment on S given by Eq. (7) is 7%.

FEM analysis

Roll and material deformation

In order to observe the material and work roll deformation during compression, three roll forces were simulated while lengthwise tension and penetration were maintained at the same values (Fig. 8). The results demonstrate that the work roll flattened before and after the contact area and deformed following a concave function along the roll gap (Fig. 8). The higher the roll force, the higher the concavity (Fig. 8b). Sun et al. [31] and Kijima [32] also found a similar deformation pattern (a concavity along the roll gap) during the skin-pass process with larger rolls diameters (500 mm) and higher roll forces ($F > 1000$ N/mm) than the one used in the HyP. Nevertheless, the concavity observed during compression at the HyP was due to the H-ASR, where a much smaller roll (the support roll) supports the normal force applied by the work roll ($R_{work\ roll}/R_{support\ roll} = 3.75$). This was verified by

Fig. 6 Comparison between HyP (a) and conventional skin-pass process (b) experimental and simulated elongation values



simulating a skin-pass FEM model under the same HyP conditions (work roll diameter of 300 mm, roll force of 200 N/mm and lengthwise tension of 20%) and observing that the resulting deformed work roll remained circular along the roll gap. To obtain a similar concave deformation, a roll force equal to 1800 N/mm was necessary, which is much higher than the maximum used in the HyP. Another similarity to the skin-pass process, was that the higher the roll force, the greater the shift toward the entry region.

Contact conditions and shear deformation

The normal pressure distributions and interfacial shear stresses along the roll gap of HyP-module 1 for different penetrations were compared to the results of an equivalent skin-pass process (Fig. 9). In the HyP, lengthwise tension and roll force were set to their medium values ($T = 20\% \sigma_{x_0}$ and $F = 150$ N/mm). For the conventional skin-pass process, two roll forces were analysed: the same roll force used for the HyP

(Fig. 9a), which provided a much smaller elongation, and a higher roll force ($F = 380$ N/mm), which provided the same elongation as the HyP (Fig. 9b).

The conventional skin-pass process results (Fig. 9a and b) concur with the work of Kijima [32] and Sun et al. [31], i.e. symmetry in the results of upper and bottom surfaces, normal pressure distribution curve centre shifted from the line of roll centres toward the entry region (the higher the roll force, the greater the shift toward the entry region) and the same signs in the interfacial shear stresses distribution curves. Regarding HyP-module 1, let us first observe the contact conditions at the upper surface (Fig. 9c) (which is the one that is imprinted by the work roll's surface). The contact length became smaller as P increases. The smaller the contact length, the higher the maximum normal pressure: given that preserving the area under the curve – which represents the roll force – is necessary (which is constant for all cases). As a result, in all cases, the normal pressure maximum value was higher than the one provided by the equivalent skin-pass process. This was also

Fig. 7 Comparison between NH-algorithm and FEM model results

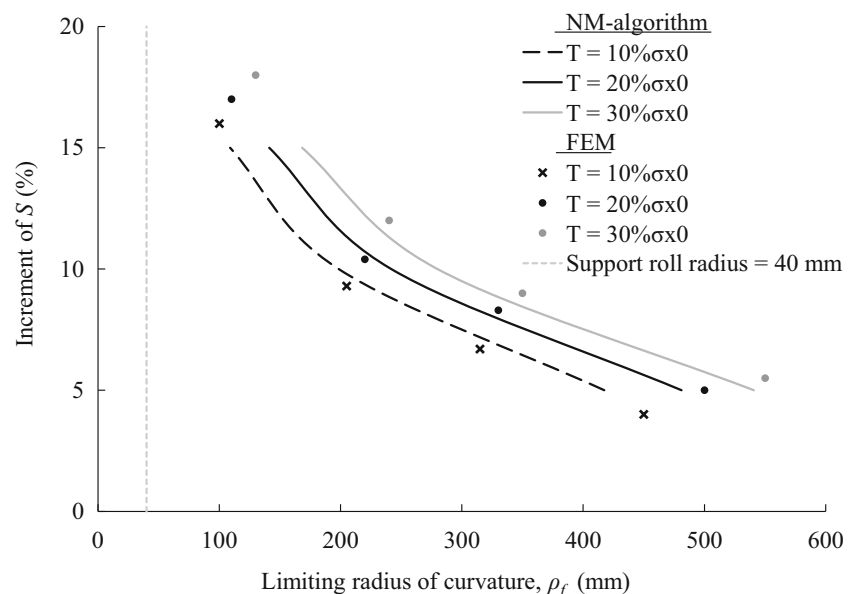


Table 3 Limiting elastic and plastic radius of curvature for different lengthwise tensions

	% Lengthwise tension (T)		
	10% σ_{x_0}	20% σ_{x_0}	30% σ_{x_0}
Displacement (β)	0.05 mm	0.10 mm	0.15 mm
Limiting elastic radius of curvature (ρ_e)	682.72 mm	744.79 mm	806.85 mm
Limiting plastic radius of curvature (ρ_p) for 10% increment on S	198.4 mm	241.7 mm	279.8 mm
Corresponding bending roll penetration (P)	22.2 mm	18.1 mm	14.8 mm

confirmed when the roll force was increased (from 150 to 380 N/mm) in the SR to attain the same final elongation (Fig. 9b). This is an advantage of ASR when using dissimilar rolls diameters, i.e. when using the same roll force, higher normal pressure is applied to the strip in an ASR than in an SR process [7]. This roll force reduction was experimentally verified in Section “Energy requirements”. In addition, as in SR, all normal pressure distribution curves’ centres shifted from the line of roll centres, and their maximum was located at the entry region. The same was observed by Hao et al. [33] for ASR: the higher the penetration, the higher the shifting. Furthermore, in all cases, the normal pressures show a “friction hill” type distribution [34], meaning that homogeneous surface deformation is dominant [35]. This represents a positive feature for consistent roughness transfer. On the other hand, as P increases, the interfacial shear stress evolves from a behaviour similar to the one observed in the SR, to an entirely opposite behaviour. This means that the frictional forces change sign as P increases.

Regarding the bottom surface (Fig. 9d), the opposite behaviour of the normal pressure is observed, i.e. as P increased the contact length became larger. And consequently, the normal pressure maximum value decreased (however it was still higher than the one observed in SR for the same roll force). In addition, the normal pressure distribution tended to a ‘double-peak’ curve as P increased. The deformation mode (‘friction hill’ or ‘double-peak’) can be predicted by the ratio of the roll-strip contact length to the initial strip thickness [35]. This ratio (q) can be approximated to: $q = R(h_0 - h_1) / h_0^2 = (\text{Reduction}) (R/h_0)$. For small values of q , a ‘double peak’ distribution is expected. On the other hand, ‘friction hill’ type pressure distribution is related to high values of q . Considering the roll diameter differences in HyP-module 1, and a maximum reduction of 2%, q is equal to 6 for the upper roll, and 1.6 for the bottom roll. This explains the different deformation modes observed in HyP-module 1. Furthermore, the shifting of the x location of the normal pressure maximum value towards the entry region is greater than in the case of the upper surface. The resulting distributions are located almost entirely at the entry region. This is due to the contact point shifting between the strip and the support roll during bending. This fact was observed

and extensively studied by Liu et al. [36]. Regarding the interfacial shear stress, the shape of the curve was constant in all cases, with two changes of sign along the curve. This behaviour was very different from that observed for the skin-pass process on the bottom surface.

The nominal friction coefficient (i.e. the interfacial shear stresses over normal pressure ratio) (Fig. 10a) for skin-pass and HyP-module 1 (with medium T , P and F values) was analysed in order to determine the slip/no-slip condition between the strip and the rolls, friction force directions, the position of neutral points (NP) and the stress state of the sheet at the roll gap. A schematic is also outlined (Fig. 10b).

Observing the results from the skin-pass process (Fig. 10a), there is a no-slip condition along the contact lengths (friction coefficient < Coulomb friction), except for a short slip region at the exit side. This was also observed by Kijima [32] for relatively small roll forces. Furthermore, because of the symmetry, there is a common position for the entrance bite point and a common neutral point for both strip surfaces. On the other hand, in HyP-module 1 (Fig. 10a), one short slip region at the exit side for the upper surface and two opposite slip regions for the bottom surface, mostly at the entry side, were recorded. In addition, asymmetry leads to different positions of the upper and bottom entrance bite points (points P1 and P2, respectively). Under these circumstances, the bottom surface would be submitted to frictional forces sooner than the upper surface at the roll-bite’s entrance (zone I), and the material in that region would show higher flow velocity than the material at the upper surface. This was also observed by Ma et al. [15] when bending the strip before rolling. Therefore, two pairs of shear forces would be generated: one in RD, producing the first cross shear region (CSR 1), and one in the normal direction (Fig. 10b). The latter is also due to the contact point between the strip and the support roll shifting toward the entry region during bending, as mentioned above [36]. Subsequently, the strip enters the deformation zone completely (zone II) and the upper and bottom surfaces reach a velocity similar to their corresponding roll surfaces (no-slip is produced), i.e. neutral points are reached, but at different x levels: first the bottom surface (NP₁) and later the upper (NP₂). Just after the bottom surface neutral point (NP₁), its interfacial

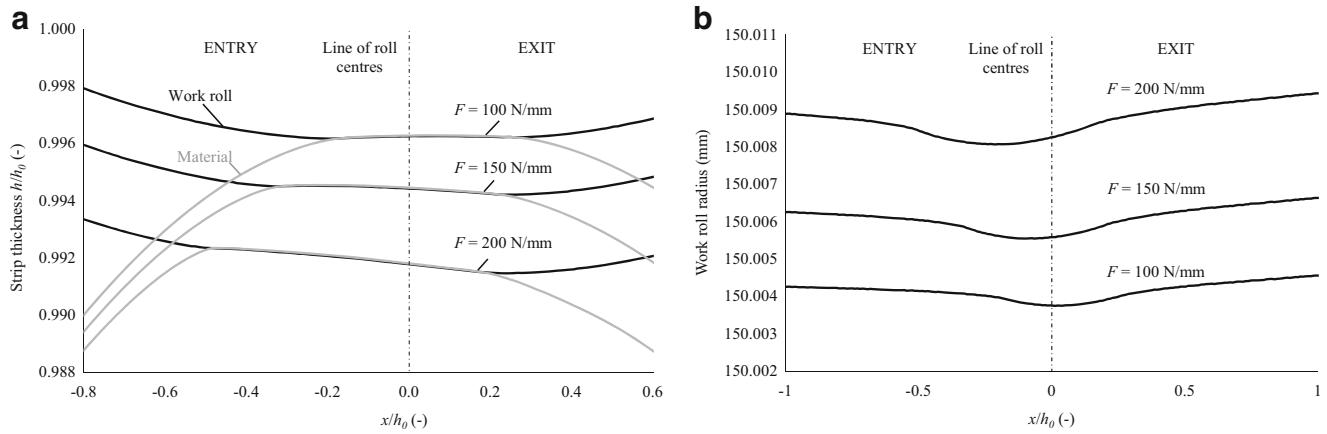


Fig. 8 Material and work roll deformation during rolling at the HyP-module 1 when different F were applied: 100, 150 and 200 N/mm. T and P were fixed to 20% σ_{x_0} and 12 mm, respectively. **(a)** Deformation at the roll gap and **(b)** work roll radius at the roll gap and surroundings

shear stresses change direction and friction forces now delay the strip motion. In addition, maximum normal stresses act on the strip introducing the necessary plastic deformation, making the desired reduction possible. Near the x level of the roll centres, the interfacial shear stress at the upper surface changed sign and the second cross shear region (CSR 2) appeared. Zone III extends to the exit side.

Accordingly, different material flow velocities at the upper and lower surfaces would be generated during rolling. As a consequence, shear deformation along the strip thickness would be expected. This was verified by the analysis of the Von Mises stress, the equivalent strain, the shear stress and the

strain rate in RD distributions along the roll gap for the skin-pass process (Fig. 11) and the HyP (Fig. 12).

As expected, in the conventional skin-pass process, the effective stresses (Fig. 11a) and the equivalent strains (Fig. 11b) were symmetrically distributed around the strip's horizontal centre line. In addition, the shear stresses (Fig. 11c) presented the typical anti-symmetrical distribution. The logarithmic strain rates in RD (Fig. 11c) has an X-like distribution, showing peak values at the entry region (due to the higher changes in the material flow velocities in this region). In all cases the registered magnitudes were lower than the ones recorded in the HyP-module 1 roll gap, except for the logarithmic strain rate in

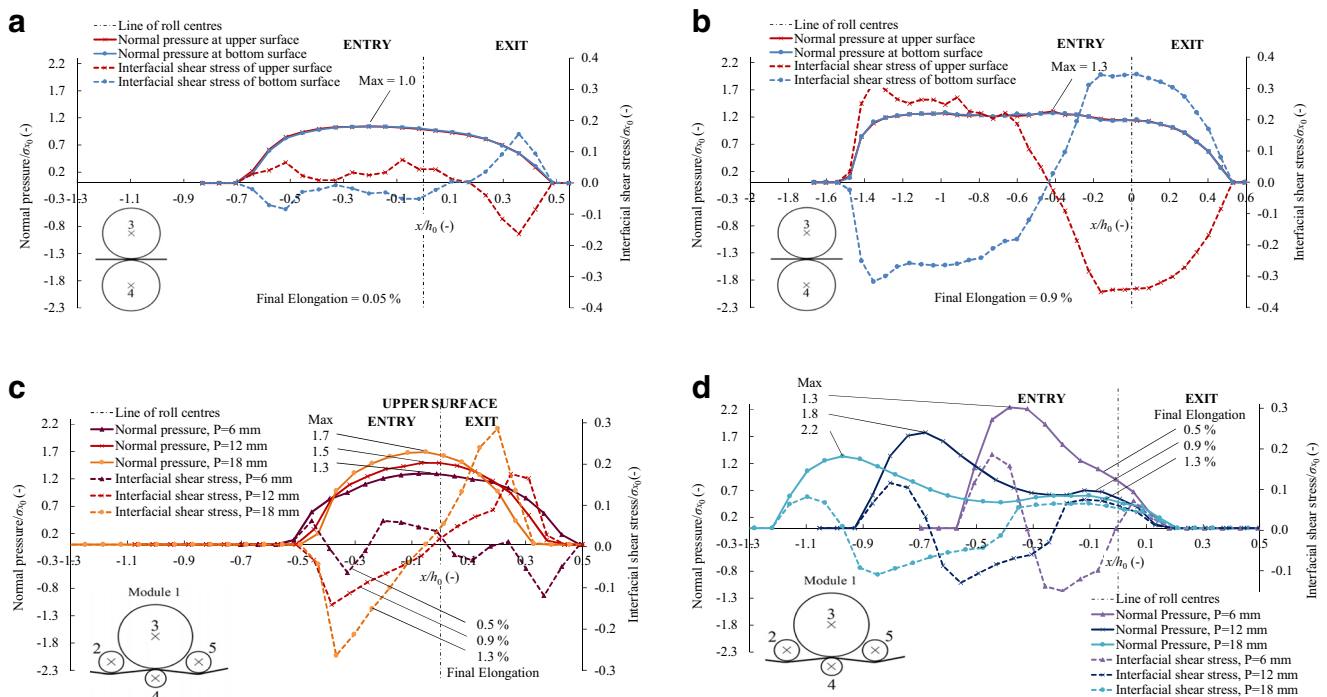


Fig. 9 Normal pressure distributions and interfacial shear stresses along the roll gap of the conventional skin-pass process for **(a)** $T = 20\% \sigma_{x_0}$ and $F = 150$ N/mm and **(b)** $F = 380$ N/mm. Same results for the HyP when

using $T = 20\% \sigma_{x_0}$, $F = 150$ N/mm and different penetrations: 6 mm, 12 mm and 18 mm for **(c)** the upper surface and **(d)** bottom surface

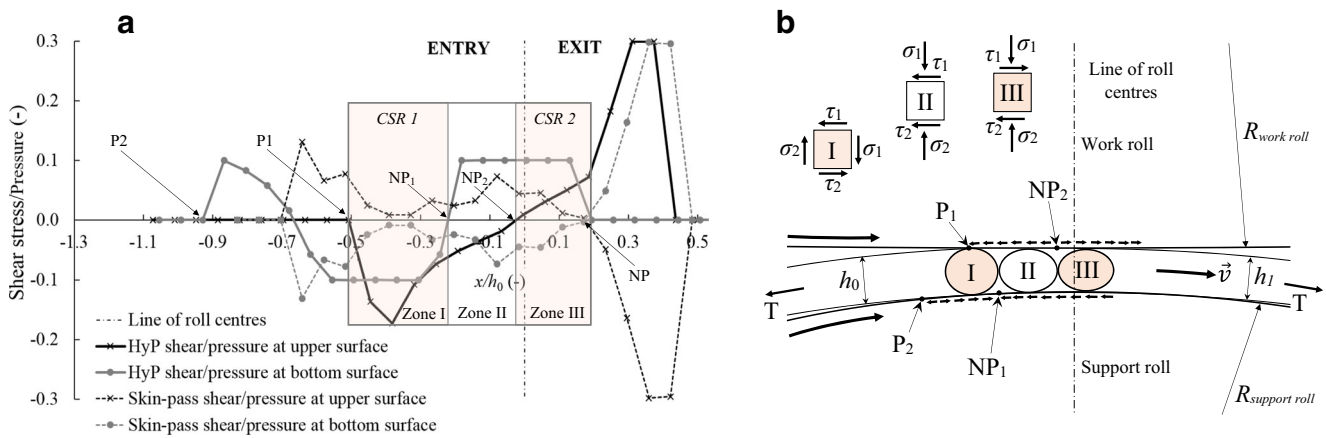


Fig. 10 Interfacial shear stresses over normal pressure ratio at upper and bottom surfaces for the skin-pass process ($T = 20\% \sigma_{x_0}$ and $F = 150 \text{ N/mm}$) and HyP-module 1 ($T = 20\% \sigma_{x_0}$, $F = 150 \text{ N/mm}$ and $P = 12 \text{ mm}$) (a) and schematic of the asymmetric rolling during HyP-module 1 (b)

RD. By contrast, the same results at the upper and lower parts of the strip when rolling with the HyP-module 1 (Fig. 12) were asymmetrically distributed. An oblique effective stress concentration band was observed (Fig. 12a), with maximum values concentrated at the upper part of the strip. In addition, the results demonstrate that the equivalent stress value for the outer fibre (upper surface) before the roll-gap is in agreement with the one predicted by the analytical model (Section “Bending limits”), with a value of 199 MPa, equivalent to an increment of 7% on the yield stress. Regarding the equivalent strain (Fig. 12b) distribution, it resembled the previous behaviour (Fig. 12a). The equivalent strain value for the outer fibre previous to the roll-gap is also shown (0.12%), indicating a small value

near yielding. Furthermore, in concordance with the “friction hill” type distribution of the normal pressure shown in Fig. 9c, a homogeneous deformation is observed at the upper surface along the roll gap (Fig. 12b). If compared to the SR, the highest equivalent strain values were shifted above the horizontal centre line. From these two contour plots (Fig. 12a and b), it was verified that the highest plastic deformation was produced at zone II. Regarding the shear stresses (Fig. 12c), the maximum tensile values were located at the roll gap entry and exit areas, specifically near the bottom entrance bite point and upper exit point, respectively. Maximum compressive stresses were located along the roll gap, following the oblique distribution previously registered. Regarding the logarithmic strain rate in RD

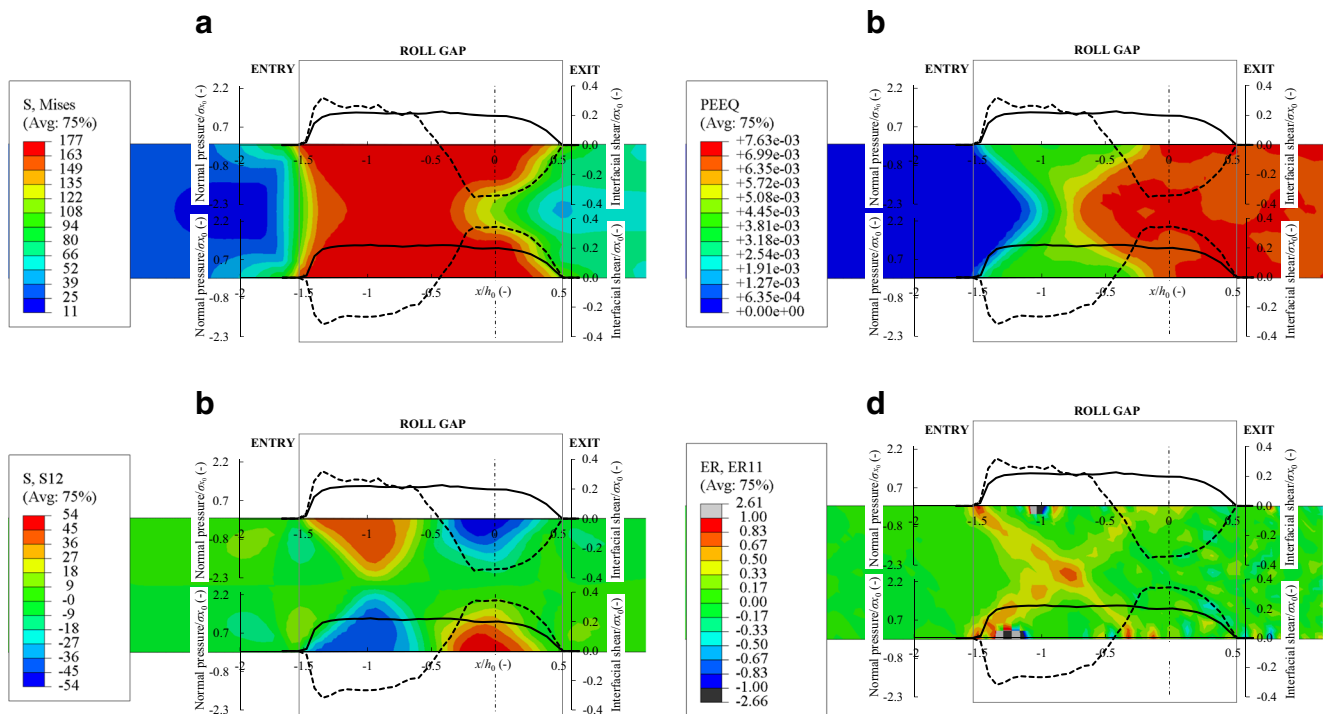


Fig. 11 Von Mises stress (S, Mises) (a), equivalent plastic strain (PEEQ) (b), shear stress (S12) (c) and logarithmic strain rate in RD (ER11) (d) distributions of skin-passed strip ($T = 20\% \sigma_{x_0}$ and $F = 380 \text{ N/mm}$). The final elongation obtained was equal to 0.9%

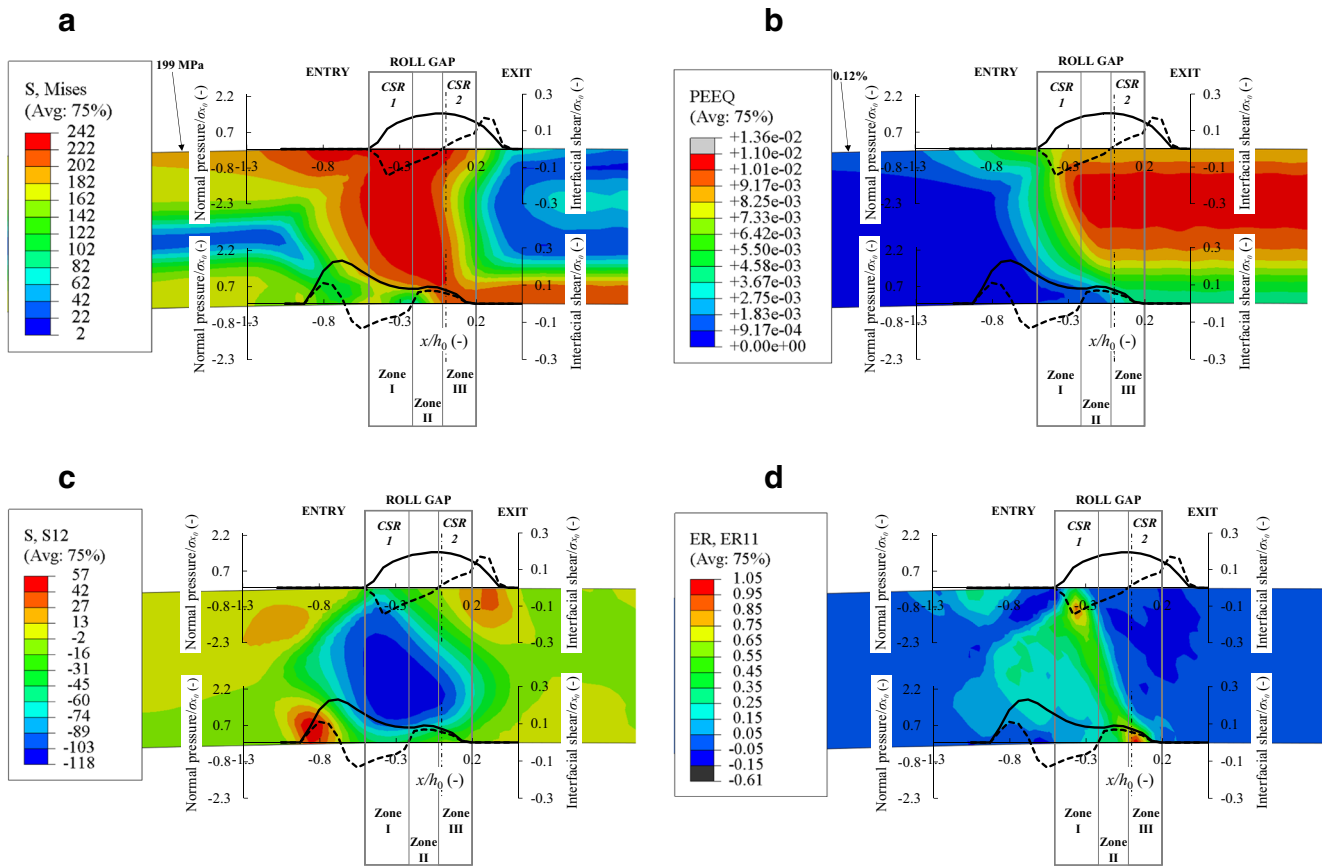


Fig. 12 Von Mises stress (S, Mises) (a), equivalent plastic strain (PEEQ) (b), shear stress (S12) (c) and logarithmic strain rate in RD (ER11) (d) distributions of strip processed by HyP-module 1 ($T = 20\% \sigma_{x_0}$, $F = 150 \text{ N/mm}$ and $P = 12 \text{ mm}$). The final elongation obtained was equal to 0.9%

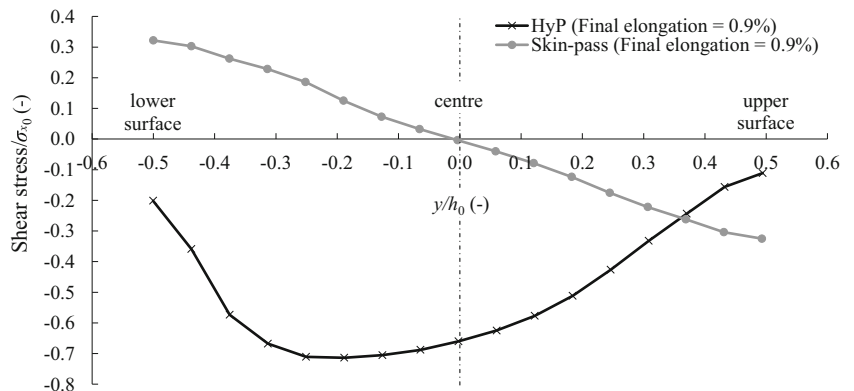
(Fig. 12d), a well-defined oblique band was observed. Furthermore, the two areas with maximum values coincided with each of the cross shear regions identified in Fig. 10 (CSR 1 and CSR 2) and were located near the strip surfaces. These results indicate the presence of shear deformations along the strip thickness introduced by the H-ASR.

For a better quantitative assessment of the differences in the through-thickness shear stresses introduced by the H-ASR and the SR, the correspondent values along a vertical line at the x level of the roll centres are depicted in Fig. 13. One can observe that H-ASR leads to higher and more heterogeneous

shear stress values than SR. In the case of SR, the shear stress reverses sign when crossing the symmetry plane. Conversely, only negative values of shear stresses were present along the strip thickness in the case of the HyP. The maximum value was in the lower half of the strip and consequently, more severe shear deformation in this part is expected.

The mesh distortion is further evidence of the shear deformation introduced by the H-ASR (Fig. 14). For more detailed observation, in Fig. 14, the grid deformation is exaggerated 100 times in RD. For the skin-passed strip, smaller deformation of the grid is observed. The vertical lines became concave

Fig. 13 Through-thickness shear stress (S12) at the middle of the roll gap for SR and H-ASR ($T = 20\% \sigma_{x_0}$, $F = 150 \text{ N/mm}$ and $P = 12 \text{ mm}$)



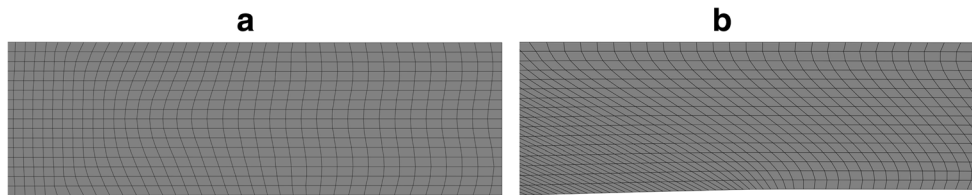


Fig. 14 Strip grid deformation at the roll gap of the skin-pass process ($T=20\% \sigma_{x_0}$ and $F=380$ N/mm) (a) and at the roll gap of the HyP-module 1 ($T=20\% \sigma_{x_0}$, $F=150$ N/mm and $P=12$ mm) (b). The grid deformation was exaggerated 100 times in RD

toward the roll-bite, turning to a double-barrel pattern afterwards. Similar deformation was also observed by Lapovok et al. [37]. In contrast to this behaviour, the rolling by the HyP-module 1 produced higher grid deformation with different inclinations of the cross section lines: counter-clockwise at the upper part of the strip and clockwise at the bottom, reflecting the shape of the stress and strain concentrations (Fig. 12a and b). Similar observations were reported by Ma et al. [15], where ASR was introduced by bending the strip. Furthermore, the through-thickness shear stress observed in Fig. 13 for the H-ASR maintains the same sign due to the superimposition of the global shear strain pattern observed in Fig. 14b.

As shown in Fig. 1, after rolling at HyP-module 1, the strip is also bent and rolled by HyP-module 2. Given that the geometric configuration of HyP-module 2 mirrors that of module 1, similar but opposite behaviours were registered. Consequently, the equivalent strain at the end of the HyP is almost symmetric (Fig. 15), guaranteeing a flat product. A similar result was found in the work of Lapovok et al. [37], where nonmonotonic ASR was achieved by flipping the sample 180 degrees around the RD. A more homogeneous state and improved formability properties were obtained by applying this kind of ASR on interstitial-free steel.

Mechanical properties

In order to verify the effect of the through-thickness shear deformation introduced by the HyP, the mechanical and formability properties of the DC04 processed strip were compared to the same material processed by an equivalent conventional finishing process (involving tension levelling and skin-pass processes).

The mechanical and formability properties after the tensile test are summarised in Table 4. The values of at least three specimens for each of the processing condition were averaged. Entry material results are also included as a reference.

As is to be expected after a rolling process, the effect of both conventional process and HyP was to increase the material strength and decrease the uniform strain and ductility compared to the characteristics of the entry material. The HyP resulting strip showed slightly lower strength than the conventional finished material. The higher increment for both processes was observed in the 45° direction, i.e. the 45° -yield stress and the 45° -tensile strength increased 35% and 22%, respectively in the conventional process, whereas the HyP increased these values by 28% and 20%, respectively. Nevertheless, on average, the HyP process generated 10% higher uniform elongation and 12% higher elongation to failure than the conventional process. In addition, the HyP increased the normal anisotropy by 53% and produced similar planar anisotropy compared to the conventional process.

Based on these results, it seems that the HyP would improve on the deep drawing properties traditionally generated by the conventional finishing process. A physical explanation for this observation could lay in the possible new grain orientation of the processed material due to the through-thickness shear deformation introduced by the H-ASR. Several authors [12–17] have proven that the through-thickness shear deformation introduced by the ASR produces a change in the microstructure and in the texture of the processed material, that have a positive influence on the material plastic behaviour, improving its drawability. To clarify this aspect regarding the H-ASR, further investigation on microstructure and texture are necessary and will be developed in future research.

Fig. 15 Equivalent plastic strain distributions of strip processed by HyP-module 2 ($T=20\% \sigma_{x_0}$, $F=150$ N/mm and $P=12$ mm)

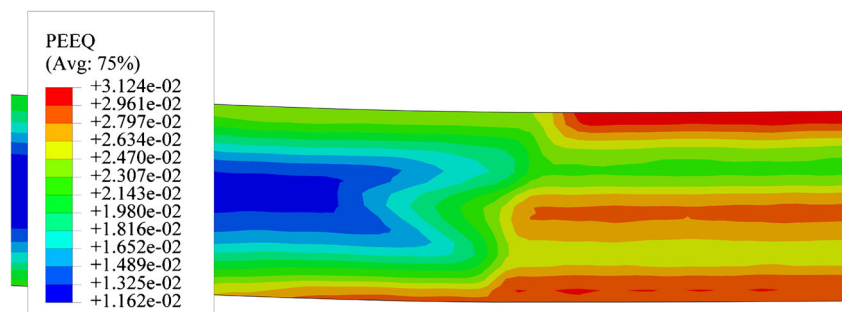


Table 4 Tensile test results for DC04 entry material (initial) and processed material by conventional finishing process and HyP

	Initial	Conventional process			HyP		
		0°	45°	90°	0°	45°	90°
Yield strength (MPa)	161.1	213.2	217.3	204.6	191.4	205.5	202.8
Ultimate tensile strength (MPa)	269.9	326.7	329.7	323.6	321.0	322.4	315.1
Uniform elongation (%)	32.4	22.9	23.1	23.0	26.1	25.2	25.46
Elongation to failure (%)	47.7	40.1	39.14	42.8	46.8	46.1	46.4
Anisotropy coefficient (r)	–	1.43	0.95	1.13	1.81	1.59	2.04
Normal anisotropy (\bar{r})		1.12			1.71		
Planar anisotropy (Δr)		0.32			0.34		

The final elongation obtained after each process was equal to 0.53%

The forming limit curves obtained from the bulge test applied on the processed materials are presented in Fig. 16. Limits for local necking and diffuse necking (following Hill's theory [38]) are also displayed.

The FLC from both specimens, under the strain tests cited in Section “Mechanical and formability properties” (tensile, biaxial-circular and biaxial-elliptical tests), are very similar to each other, indicating comparable behaviour under these biaxial loads.

The Erichsen index (obtained from the Erichsen cupping test) from the conventionally finished material was 11.3, and 12.4 from the material processed by the HyP. Therefore, the steel sheet obtained by the HyP exhibited 10% better ductility (in the plane of drawing under biaxial stress conditions) than the conventionally manufactured material.

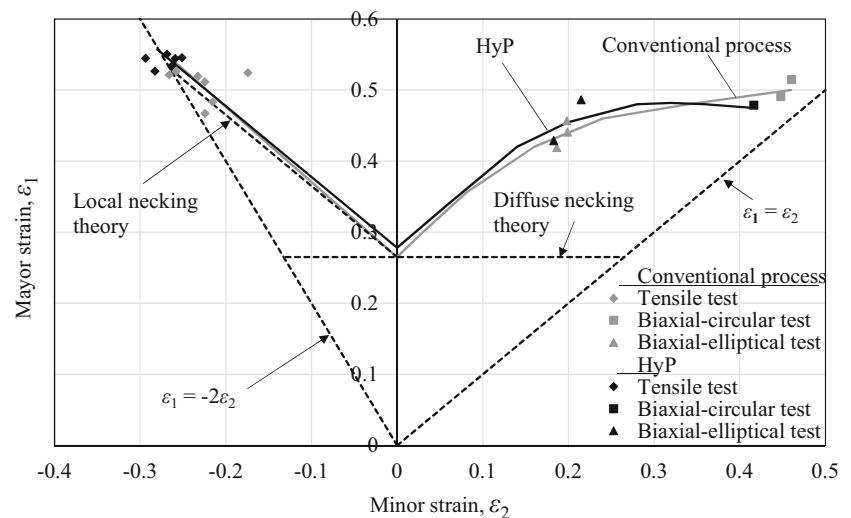
Based on these tensile and formability tests results, it appears that HyP produces sheets with better drawability, satisfactory strength, and formability qualities comparable to the conventional finishing process. As stated before, these results concur with the observations of several researchers that have studied different ASR processes [10, 14–20]. All these

authors agree that the introduction of shear deformation along the strip thickness during ASR produces a new microstructure (with a different grain orientation) that improves the mechanical properties and formability characteristics of the processed material. As mentioned previously, further investigation into this aspect of materials processed by the HyP is necessary and will be undertaken in future research.

Energy requirements

As stated before, the analysis of energy requirement was based on the roll force and power used by the HyP when achieving the same final elongation as the conventional finishing process. To have a general idea, we specifically focused on points 1, 2 and 3 of the experimental elongation versus roll force curves (Figs. 3 and 4) for medium values of lengthwise tension and penetration (Fig. 17). The results indicate that a drastic rolling force reduction, up to 63%, could be achieved using the HyP. This finding verifies one of the advantages of applying asymmetrical rolling.

Fig. 16 Forming limit curves from DC04 material processed by conventional process and by HyP



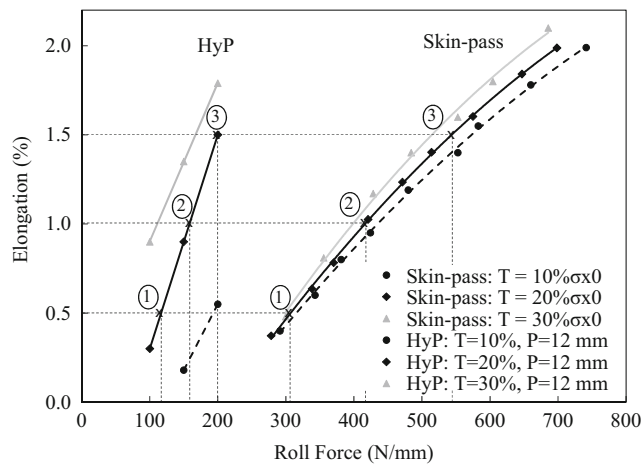


Fig. 17 Experimental relationship between rolling force and elongation for the HyP and the skin-pass. Points 1, 2 and 3 are used for the analysis of energy requirement

To compare both processes, in terms of power required to deform the material along the roll gap, rolling torques applied by the H-ASR and the SR process to achieve a final elongation of 0.9% were calculated. The interfacial shear stress curves obtained by the FEM models were used. Thus, the interfacial shear stress curves of Fig. 9b, for the SR, and Fig. 9c–d, for the H-ASR, were integrated. From the specification of both processes we find that $R_1 = R_2 = 300$ mm, for the SR and $R_1 = 300$ mm and $R_2 = 40$ mm, for the H-ASR. The strip linear velocity was set to 2.4 m/min. Therefore, $\omega_1 = \omega_2 = 0.267$ rad/s for the SR process and $\omega_1 = 0.267$ rad/s mm and $\omega_2 = 1$ rad/s, for the H-ASR. Using Eqs. (9)–(12), Table 5, was obtained.

For this elongation (0.9%), the results indicate that the HyP requires 55% less power than the conventional process to deform the strip. Therefore, a considerable energy reduction could be achieved by using the HyP.

Conclusions

A novel steel strip finishing process, the HyP, which combines skin-pass and tension levelling into one production step was

Table 5 Rolling torques and power required to deform the material along the roll gap when using the HyP and the conventional process to achieve a final elongation of 0.9%

	Conventional process	HyP
T_1	- 0.108 N·m/mm	+ 0.040 N·m/mm
T_2	+ 0.108 N·m/mm	- 0.015 N·m/mm
$T = T_1 + T_2 $	0.216 N·m/mm	0.055 N·m/mm
P_1	0.029 W/mm	0.011 W/mm
P_2	0.029 W/mm	0.015 W/mm
$P = P_1 + P_2$	0.058 W/mm	0.026 W/mm

analysed by means of FEM models and experimental results. The validation of the FEM models was based on experiments at the pilot facility and industrial trials. An analytical model used to predict the appropriate bending limits for the HyP was provided. The analysis of energy requirement, based on the roll force and power used by the HyP to achieve the same final elongation as the conventional finishing process, revealed that a drastic energy reduction, up to 63% on rolling force and 55% on power, could be achieved using the HyP. In addition, it is expected that 25% to 30% less space would be needed for its industrial implementation than for a typical finishing layout. The material deformation, contact conditions and stress state during rolling were investigated and compared to the corresponding results from a traditional skin-pass process. Due to the differences in compressional roll diameters ($R_{work\ roll}/R_{support\ roll} = 3.75$) and the bending of the strip before the entrance of the roll gap, the HyP presented asymmetric conditions during rolling (H-ASR). Contact conditions along the first roll gap (HyP-module 1) showed a “friction hill” normal pressure distribution over the upper surface with a higher maximum value. This would facilitate a consistent roughness transfer over this surface, while using a lower roll force as compared to a conventional skin-pass process. In addition, the H-ASR generated two cross shear zones during rolling, where opposite shear stresses were observed. The FEM results also showed that the H-ASR introduced higher shear deformation along the strip thickness than a conventional SR. The positive influence of the through-thickness shear deformation during H-ASR was verified by tensile and formability tests conducted on specimens processed by the HyP pilot facility. The results indicate that the HyP produces steel sheets with better drawability, satisfactory strength and formability qualities comparable to the conventional finishing process. Finally, a methodology based on hard and soft computing, to find the optimal HyP parameter combination (T , P and F) that guarantee the required elongation, minimizing residual stresses magnitude and imbalance in the final product will be undertaken in future research.

Acknowledgements The authors would like to express their gratitude for the financial support provided by the European Union, under the RFCS project reference RFSR-CT-2007-00016, which has made this research possible. Special thanks to U. Weirauch Engr. and K. Boguslawsky Engr., both from Andritz Sundwig GmbH (Hemer, Germany), for their invaluable dedication in building the HyP pilot facility and for their subsequent assistance. The authors would also like to thank G. Zwickel Engr. and M. Ullrich Engr., both from Bilstein Group GmbH (Hagen, Germany), for providing the extremely valuable skin-pass process experimental data. We would also like to express our gratitude to H. Gouveia PhD. from ISQ (Porto Salvo, Portugal) for the tests conducted on the processed materials. One of the authors (JFC) would also like to acknowledge the University of La Rioja for the FPI fellowship program. Finally, we would like to add that this work used the Beronia cluster (Universidad de La Rioja), which is supported by FEDER-MINECO grant number UNLR-094E-2C-225.

Funding This study was funded by the European Union, under the RFCS project reference RFSR-CT-2007-00016.

Compliance with ethical standards

Conflict of interest The authors declare that they have no conflict of interest.

References

- Mapelli C, Barella S, Mombelli D, Baldizzone C, Gruttadauria A (2013) Comparison between symmetric and asymmetric hot rolling techniques performed on duplex stainless steel 2205. *Int J Mater Form* 6(3):327–339. <https://doi.org/10.1007/s12289-011-1089-9>
- Wiklund O, Sandberg F (2002) Modelling and control of temper rolling and skin pass rolling. In: Lenard JG (ed) *Metal forming science and practice*. Elsevier, Oxford, pp 313–343. <https://doi.org/10.1016/B978-008044024-8/50015-1>
- Morris JW, Hardy SJ, Thomas JT (2002) Some fundamental considerations for the control of residual flatness in tension levelling. *J Mater Process Technol* 120(1–3):385–396. [https://doi.org/10.1016/S0924-0136\(01\)01175-X](https://doi.org/10.1016/S0924-0136(01)01175-X)
- Abdelkhalek S, Zahrouni H, Potier-Ferry M, Legrand N, Montmitonnet P, Buessler P (2009) Coupled and uncoupled approaches for thin cold rolled strip buckling prediction. *Int J Mater Form* 2(SUPPL. 1):833–836. <https://doi.org/10.1007/s12289-009-0547-0>
- Diegelmann V, Zwickel G, Ullrich M, Gouveia H, Weirauch U, Boguslawsky K, Pernía-Espinoza A (2013) Neues Verfahren zur unabhängigen Einstellung der mechanischen und topografischen Bändeigenschaften. *Stahl und Eisen* 133(11):215–222
- Gorelik VS, Klimenko IV (1997) Classification and analysis of processes of plate/strip rolling with asymmetric deformation zone. *Russ Metall* 3:34–42
- Hwang Y-M, Tzou G-Y (1997) Analytical and experimental study on asymmetrical sheet rolling. *Int J Mech Sci* 39(3):289–303. [https://doi.org/10.1016/S0020-7403\(96\)00024-0](https://doi.org/10.1016/S0020-7403(96)00024-0)
- Wronski S, Bacroix B (2014) Microstructure evolution and grain refinement in asymmetrically rolled aluminium. *Acta Mater* 76:404–412. <https://doi.org/10.1016/j.actamat.2014.05.034>
- Ma C, Hou L, Zhang J, Zhuang L (2016) Influence of thickness reduction per pass on strain, microstructures and mechanical properties of 7050 Al alloy sheet processed by asymmetric rolling. *Mater Sci Eng A* 650:454–468. <https://doi.org/10.1016/j.msea.2015.10.059>
- Yang J, Li S, Liu J, Li X, Zhang X (2017) Finite element analysis of bending behavior and strain heterogeneity in snake rolling of AA7050 plates using a hyperbolic sine-type constitutive law. *J Mater Process Technol* 240:274–283. <https://doi.org/10.1016/j.jmatprotec.2016.10.009>
- Zhang SH, Zhao DW, Gao CR, Wang GD (2012) Analysis of asymmetrical sheet rolling by slab method. *Int J Mech Sci* 65(1):168–176. <https://doi.org/10.1016/j.ijmecsci.2012.09.015>
- Shore D, Kestens LAI, Sidor J, van Houtte P, van Bael A (2016) Process parameter influence on texture heterogeneity in asymmetric rolling of aluminium sheet alloys. *Int J Mater Form*:1–13. <https://doi.org/10.1007/s12289-016-1330-7>
- Ouali MO, Aberkane M (2008) Multiscales modeling of microstructure evolution during asymmetric cold rolling process. *Int J Mater Form* 1(SUPPL. 1):89–92. <https://doi.org/10.1007/s12289-008-0039-7>
- Cai M, Wei X, Rolfe B, Hodgson PD (2015) Microstructure and texture evolution during tensile deformation of symmetric/asymmetric-rolled low carbon microalloyed steel. *Mater Sci Eng A* 641:297–304. <https://doi.org/10.1016/j.msea.2015.06.062>
- Ma R, Wang L, Wang YN, Zhou DZ (2015) Microstructure and mechanical properties of the AZ31 magnesium alloy sheets processed by asymmetric reduction rolling. *Mater Sci Eng A* 638(0):190–196. <https://doi.org/10.1016/j.msea.2015.03.093>
- Toth LS, Beausir B, Orlov D, Lapovok R, Haldar A (2012) Analysis of texture and R value variations in asymmetric rolling of IF steel. *J Mater Process Technol* 212(2):509–515. <https://doi.org/10.1016/j.jmatprotec.2011.10.018>
- Hamad K, Chung BK, Ko YG (2014) Microstructure and mechanical properties of severely deformed mg–3%al–1%Zn alloy via isothermal differential speed rolling at 453 K. *J Alloys Compd* 615(Supplement 1(0)):S590–S594. <https://doi.org/10.1016/j.jallcom.2013.12.195>
- Duan Y, Xu G, Tang L, Liu Y, Xu J, Deng Y, Yin Z (2017) Excellent high strain rate superplasticity of Al–Mg–Sc–Zr alloy sheet produced by an improved asymmetrical rolling process. *J Alloys Compd* 715:311–321. <https://doi.org/10.1016/j.jallcom.2017.04.273>
- Li S, Qin N, Liu J, Zhang X (2016) Microstructure, texture and mechanical properties of AA1060 aluminum plate processed by snake rolling. *Mater Des* 90:1010–1017. <https://doi.org/10.1016/j.matdes.2015.11.054>
- Guo X, Deng Y, Zhang Y, Zhang J, Zhang X (2017) Microstructure and microtexture evolution of shear bands in Al–Cu single crystal during asymmetric rolling. *Mater Charact* 128:37–42. <https://doi.org/10.1016/j.matchar.2017.03.022>
- Nakhoul R, Montmitonnet P, Legrand N (2015) Manifested flatness defect prediction in cold rolling of thin strips. *Int J Mater Form* 8(2):283–292. <https://doi.org/10.1007/s12289-014-1166-y>
- Kijima H, Bay N (2007) Contact conditions in skin-pass rolling. *CIRP Ann Manuf Technol* 56(1):301–306. <https://doi.org/10.1016/j.cirp.2007.05.070>
- Szucs M, Krallics G, Lenard JG (2017) The stribeck curve in cold flat rolling. *Int J Mater Form* 10(1):99–107. <https://doi.org/10.1007/s12289-015-1263-6>
- Escribano R, Lostado R, Martínez-de-Pisón FJ, Pernía A, Vergara E (2012) Modelling a skin-pass rolling process by means of data mining techniques and finite element method. *J Iron Steel Res Int* 19(5):43–49. [https://doi.org/10.1016/S1006-706X\(12\)60098-3](https://doi.org/10.1016/S1006-706X(12)60098-3)
- Marciniak Z, Duncan JL, Hu SJ (2002) 10-Combined bending and tension of sheet. In: *Mechanics of sheet metal forming*, 2nd edn. Butterworth-Heinemann, Oxford, pp 136–151. <https://doi.org/10.1016/B978-075065300-8/50013-3>
- Roberts J, Sheppard T (1971) On the mechanics of the tension-levelling process. *J Inst Met* 99:293–301
- Byrd RH, Lu PH, Nocedal J, Zhu CY (1995) A limited memory algorithm for bound constrained optimization. *SIAM J Sci Comput* 16(5):1190–1208. <https://doi.org/10.1137/0916069>
- Montgomery D (2001) *Design and analysis of experiments*, 5th edn. John Wiley and Sons, INC., New York
- Corporation DSS (2011) *ABAQUS User's Manual* 6.11. Providence
- Banabic D (2007) *Advanced methods in material forming*. Springer-Verlag Berlin Heidelberg Berlin. <https://doi.org/10.1007/3-540-69845-0>
- Sun J-N, Huang H-G, Du F-S, Li X-T (2009) Nonlinear finite element analysis of thin strip temper rolling process. *J Iron Steel Res Int* 16(4):27–32. [https://doi.org/10.1016/S1006-706X\(09\)60056-X](https://doi.org/10.1016/S1006-706X(09)60056-X)
- Kijima H (2013) Influence of roll radius on contact condition and material deformation in skin-pass rolling of steel strip. *J Mater Process Technol* 213(10):1764–1771. <https://doi.org/10.1016/j.jmatprotec.2013.04.011>
- Hao L, Di H-S, Gong D-Y (2013) Analysis of sheet curvature in asymmetrical cold rolling. *J Iron Steel Res Int* 20(5):34–37. [https://doi.org/10.1016/S1006-706X\(13\)60094-1](https://doi.org/10.1016/S1006-706X(13)60094-1)
- Beik HAA, Dehghani K (2008) Irregularity in friction hills during the cold rolling of materials. *Int J Mater Form* 1(SUPPL. 1):343–346. <https://doi.org/10.1007/s12289-008-0065-5>

35. Kobayashi S, Oh S, Altan T (1989) Metal forming and the finite-element method. Oxford series on advanced manufacturing. Oxford University Press, New York
36. Liu Z, Wang Y, Yan X (2012) A new model for the plate leveling process based on curvature integration method. *Int J Mech Sci* 54(1):213–224. <https://doi.org/10.1016/j.ijmecsci.2011.10.011>
37. Lapovok R, Orlov D, Timokhina IB, Pougis A, Toth LS, Hodgson PD, Haldar A, Bhattacharjee D (2012) Asymmetric rolling of interstitial-free steel using one idle roll. *Metall Mater Trans A Phys Metall Mater Sci* 43(4):1328–1340. <https://doi.org/10.1007/s11661-011-0960-0>
38. Hill R (1952) On discontinuous plastic states, with special reference to localized necking in thin sheets. *J Mech Phys Solids* 1(1):19–30. [https://doi.org/10.1016/0022-5096\(52\)90003-3](https://doi.org/10.1016/0022-5096(52)90003-3)